



UNICA

UNIVERSITÀ
DEGLI STUDI
DI CAGLIARI



Università di Cagliari

UNICA IRIS Institutional Research Information System

This is the Author's submitted manuscript version of the following contribution:

G. Satta, M. Trajkovski, A. Cantara, M. Mura, C. Meloni, G. Olla, M. Dobrovolná, L. Pisano, S. Gaspa, A. Salis, L. De Luca, F. Mocci, V. Brazda, J. Plavec, and M. Carraro, Complex Biophysical and Computational Analyses of G-Quadruplex Ligands: The Porphyrin Stacks Back *Chem. Eur. J.* **2024**, e202402600.

The publisher's version is available at:

<https://doi.org/10.1002/chem.202402600>

When citing, please refer to the published version.

This full text was downloaded from UNICA IRIS <https://iris.unica.it/>

Complex Biophysical and Computational Analyses of G-Quadruplex Ligands: The Porphyrin Stacks Back

Giuseppe Satta^{[a],[b]}, Marko Trajkovski^[c], Alessio Cantara^[d], Monica Mura^[e], Claudia Meloni^[e], Giulia Olla^[e], Michaela Dobrovolná^[d], Luisa Pisano^{[a],[b]}, Silvia Gaspa^[a], Andrea Salis^[e], Lidia De Luca^[a], Francesca Mocci^[e], Vaclav Brazda^[d], Janez Plavec^{*[c],[f],[g]}, Massimo Carraro^{*[a],[b]}

[a] Dr. G. Satta, Dr. L. Pisano, Dr. S. Gaspa, Prof. Dr. L. De Luca, Dr. M. Carraro
Department of Chemical, Physical, Mathematical and Natural Sciences,
University of Sassari,
Via Vienna 2, Sassari, 07100, Italy
E-mail: mcarraro@uniss.it

[b] Dr. G. Satta, Dr. L. Pisano, Dr. M. Carraro
Consorzio Interuniversitario Reattività Chimica e Catalisi (CIRCC),
Via Celso Ulpiani 27, Bari, 70126, Italy

[c] Dr. M. Trajkovski, Prof. Dr. J. Plavec
Slovenian NMR Centre,
National Institute of Chemistry,
Ljubljana SI-1000, Slovenia,
E-mail: janez.plavec@ki.si

[d] Dr. A. Cantara, M. Dobrovolná, Prof. Dr. V. Brazda
Institute of Biophysics,
Czech Academy of Sciences,
Královopolská 135, 612 65 Brno, Czech Republic

[e] M. Mura, C. Meloni, G. Olla, Prof. Dr. A. Salis, F. Mocci
Department of Chemistry and Geological Science,
University of Cagliari,
Cittadella Universitaria, I-09042 Monserrato, Italy

[f] Prof. Dr. J. Plavec
EN→FIST Centre of Excellence,
Trg OF 13, SI-1000 Ljubljana, Slovenia

[g] Prof. Dr. J. Plavec
Faculty of Chemistry and Chemical Technology,
University of Ljubljana,
Vecna pot 113, SI-1000 Ljubljana, Slovenia

Supporting information for this article is given via a link at the end of the document.

Abstract: G-quadruplexes (G4s), as non-canonical DNA structures, attract a great deal of research interest in the molecular biology as well as in the material science fields. The use of small molecules as ligands for G-quadruplexes has emerged as a tool to regulate gene expression and telomeres maintenance. *Meso*-tetrakis-(*N*-methyl-4-pyridyl)porphyrin (TMPyP4) was shown as one of the first ligands for G-quadruplexes and it is still widely used. We report an investigation comprising molecular docking and dynamics, synthesis and multiple spectroscopic and spectrometric determinations on simple cationic porphyrins and their interaction with different DNA sequences. The study allowed to synthesize a few compounds that have shown to interact with DNA; the detailed characterization has shown that the presence of amide groups at the periphery improves selectivity for parallel G4s binding over other structures. Taking into account the ease of synthesis, 5,10,15,20-tetrakis-(1-acetamido-4-pyridyl)porphyrin bromide could be considered a better alternative to TMPyP4 in studies involving G4 binding.

Introduction

Several genomic regions are characterized by a relative abundance of guanine. The large amount of guanine units, in the presence of monovalent cations such as K^+ and Na^+ , allows their folding and leads to the formation of planar tetrads called G-quartets, together by a network of hydrogen bonds through Hoogsteen base pairing^[1,2]. Stacking of G-quartets, stabilized by the coordination of the monovalent metal ion with the O6 oxygen of guanines, leads to the formation of "non-canonical" structures, characterized by a four chains helical structure, called G-quadruplexes (G4). The presence of G4 in telomeres and several other non-coding regions of genome have been associated with a variety of regulatory functions. The human telomere is approximately 5,000 to 8,000 base pairs in length and features a single-stranded 3' overhang ranging from 100 to 200 bases^[1]. This overhang is primarily composed of the repetitive TTAGGG sequence. Most healthy cells possess a limited capacity for division, as was demonstrated by Hayflick and Moorhead in 1961^[3]. It is currently known that this effect is related to telomere length, which act as biological clocks that, after reaching a limiting length, trigger the senescence process^[4]. A problem often correlated with the presence of tumor activity is abnormal cellular proliferation, which in most cases, is associated with the overexpression of telomerase activity^[5]. This enzyme, a reverse cellular transcriptase, regulates telomere elongation, thereby preserving its integrity. A correlation has been assessed between telomere length maintenance and the cellular ability, typical of cancer cells, to escape replicative senescence, and in fact more than 90 percent of cancer cells show telomerase enzyme activity^[6]. The fact that most healthy cells are telomerase-silent while there is its overexpression in cancer cells, makes this enzyme an attractive target for post-diagnosis treatments. The inhibition of telomerase can be achieved either through small molecules that bind directly to the

enzyme^[7,8] or by stabilizing G4 structures. The latter method involves the use of ligands that bind to and stabilize G4 structures, which act as physiological blocks to the telomerase's ability to code and extend telomeres^[9]. G4 can also be found in oncogene promoters, replication initiation sites and untranslated regions, showing their biological relevance^[10–12]. For example, the *c-Myc* gene plays an essential role in the regulation of cell growth, proliferation, and apoptosis. When over-expressed or mutated, as in cancer cells, this gene can drive cells toward uncontrolled proliferation and thus contribute to the formation of various types of cancer^[13]. Within its sequence, the *c-Myc* proto-oncogene possesses the nuclear hypersensitivity element III₁ (NHEIII₁) region which has been shown to be highly influential in the regulation of this gene^[14]. Stabilizing this structure with ligands was noted to suppress further transcriptional activation of the *c-Myc* gene^[15]. G4 can be unimolecular or intermolecular. Depending on the orientation of the chains, they can adopt different topologies^[16] (Figure 1), influenced by factors such as molecular crowding^[17,18] and nature of monovalent cation^[19]. Furthermore, the structural and biochemical features of G4s, prompted their use in biosensors^[20] and nanomaterials^[21,22].

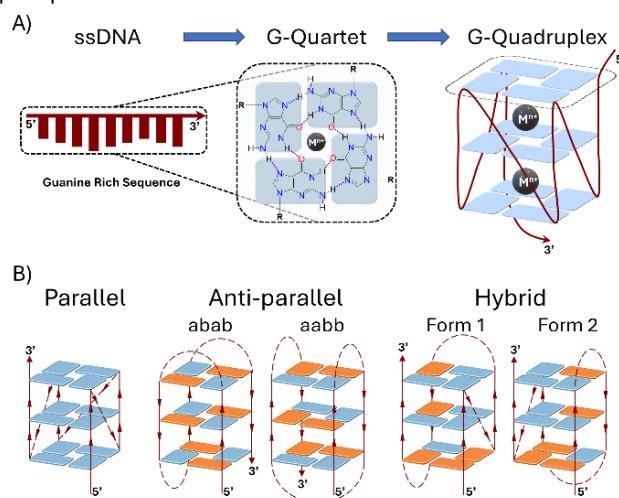


Figure 1. (A) structure of the G-quartet formed by Hoogsteen base pairing of four guanine residues and piling up to give G4. (B) Schematic intramolecular topologies of G4 structures. Blue and orange rectangles depict guanines exhibiting *syn* and *anti* conformation of glycosidic torsion angle, respectively.

The study of G4 ligands has thus become a productive field of research^[23–32]. Basically, there are 4 ways in which a ligand can interact with a G4: stacking on top or bottom G-quartets, intercalation between them, interaction with loops, or a combination of these ways. Electron-deficient cores promote interactions through π - π stacking, while cationic portions on substituents determine electrostatic interactions with negative charged phosphodiester groups, and so on^[33]. These considerations led to the discovery of various types of ligands, among others porphyrins: natural derivatives include Fe(III)-protoporphyrin IX^[34], while the first synthetic derivative is 5,10,15,20-tetrakis-(*N*-methyl-4-pyridyl)porphyrin (TMPyP4), whose activity as telomerase inhibitor was demonstrated by

Wheelhouse et al. in 1998^[35]. **TMPyP4** has been shown also to reduce the expression of the proto-oncogene c-Myc and several c-Myc-regulated genes that contain G4-forming sequences. This modulation led to in vivo antitumor effects in various models, including the ability to inhibit tumor growth and prolong survival^[36]. **TMPyP4**, has become a staple between ligands used in G4 studies but displayed a limited selectivity^[37], prompting to the development of various derivatives with demanding synthesis^[38–41]. In this work, several simple porphyrin derivatives with potential binding and stabilizing activity toward G4 were screened through a molecular modelling procedure, which included docking and molecular dynamics. Simulations were conducted on different G4 comprising one from the human telomeric sequence with a parallel topology (PDB ID:1KF1^[42]) and another present in the NHEIII₁ region of the c-Myc proto-oncogene, also known to have a parallel propeller type topology (PDB ID: 1XAV^[43]). The results of the docking procedure guided in the choice of the derivatives to be synthesized and subjected to various stability and binding studies. Specifically, a derivative of 5,10,15,20-tetrakis-4-pyridylporphyrin (**TPyP**) with amidomethyl substituent was found to be the most promising, and its properties are here compared with those of well-known porphyrin derivative, **TMPyP4**. One of the focuses of the work was to assess whether substituting the methyl groups of **TMPyP4** affect its interaction with G4 from telomere and c-Myc. This comparison was made by evaluating the results obtained for the substituted derivatives alongside those obtained for **TMPyP4** using NMR spectroscopy and mass spectrometry. NMR spectroscopy has proven to be a very versatile technique for assessing the formation of a complex, and providing crucial insights into the mode of ligand/G4 interaction. In particular NOESY and ROESY experiments^[43–45], have been employed for structural assessment of the complexes and identification of the corresponding G4-ligand interfaces. The stability of the ligand/G4 complexes was evaluated by mass spectrometry,^[46–48] specifically, with MS/MS technique: the intensity of isolated molecular ion generated by the porphyrins/G4 complex was measured as a function of increasing collision energy in the analyzer. Porphyrin derivatives were then subjected to some preliminary tests to evaluate their cytotoxicity on breast cancer (MCF-7) and Human Dermal Fibroblast (HDF) cell lines. Main Text Paragraph.

Results and Discussion

In this work, the interaction between tetracationic porphyrins derivatives and different DNA G4s was evaluated. Proposed ligand structures are reported in Table 1. **TMPyP4**, chosen as literature reference ligand, and designed ligands, **PL1** to **PL7**, were first subjected to molecular docking calculations on different G4 structures. Most promising ligands were then synthesized, and their G4 binding abilities studied by UV and NMR spectroscopies and mass spectrometry. Chosen

sequences were derived from the NHEIII₁ region of the c-Myc proto-oncogene, and the human telomeres.

Molecular Docking

The GScore values for the best poses obtained for the studied ligands on the studied G4s are reported **Table 2**. According to the docking results obtained on all-parallel G4 1XAV and 1KF1, candidates **PL3**, **PL6** and **PL7** were the most promising. Unfortunately, the synthesis of **PL3** proved to be challenging. Given that **PL6** and **PL7** exhibited a comparable G4 affinity to that showed by **PL3**, the synthesis of the latter was not pursued further. It was observed that both **PL6** and **PL7** demonstrated binding ability to other topologies in addition to the all-parallel ones. However, given the absence of stereocenters and the lower molecular weight, **PL7** was selected for further computational studies.

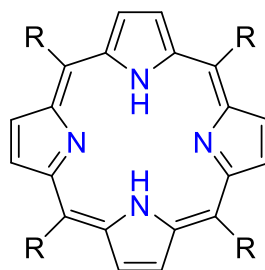


Figure 2. Porphyrin general core. R groups indicate *meso* substituents.

Table 1. Proposed porphyrin ligands *meso* substituents

Ligands	Ligands' <i>meso</i> substituents (R)	MW
TMPyP4		678.84
PL1		943.07
PL2		943.07
PL3		1115.75
PL4		911.16

PL5		850.83
PL6		907.05
PL7		850.94
PL7-Me		907.05
PL7-2Me		963.16

Table 2. XP GScore.

Ligands	1XAV ^[a]	1KF1 ^{[b][f]}	2JPZ ^[c]	2HY9 ^[d]	143D ^[e]
TMPyP4	-13,50	np ^[g]	np	np	np
PL1	-14,11	-14,63	- ^[h]	-	np
PL2	-14,77	-14,16	-	-	-12,79
PL3	-17,84	-19,14	-	-	-14,70
PL4	-9,89	-15,77	-	-	np
PL5	-14,07	-14,28	np	-14,09	-
PL6^[i]	-17,74	-19,12	-15,29	-15,36	-
PL7	-18,69	-18,66	-18,21	-16,79	-14,81

G4 names correspond to PDB ID. [a] Main G4 forms in the c-MYC promoter gene. [b] Human telomeric parallel G4. [c] Human telomeric hybrid-form 1 G4. [d] Human telomeric hybrid-form 2 G4. [e] Human telomeric antiparallel G4. [f] All G4 structures were determined in solution by NMR except for 1KF1 (X-Ray

solid structure). [g] np: no poses were found. [h] the dash symbol indicates that the docking was not performed. [i] Configuration of the chiral centers of ligand **PL6** in the best pose: SRSR,SSSS, SRRS,SSSS.

Molecular Dynamics Simulations

To investigate the impact of **PL7** on the stability of G4, a series of molecular dynamics (MD) simulations were conducted. The system was simulated in a water solution using 1KF1 as G4, both in the presence and absence of the ligand. For the complex **PL7/G4**, the structure obtained from molecular docking studies was used. Simulations were conducted at temperatures of 300, 500, 550 and 525 K, to induce denaturation. Experimentally, the process of thermal denaturation is observed to occur over a timescale that is too long to be replicated within the constraints of reasonable timescales in silico. The use of higher temperatures than those measured in real laboratory experiments has been found to accelerate the denaturation process and make it occur within accessible timescales for MD simulations.^[49–51] It is important to note that this approach is feasible due to the harmonic potentials of the force field, which prevent significant deviations in bond length or bond breakage even at elevated temperatures. Furthermore, previous studies have demonstrated that increasing temperature does not alter the denaturation pathway^[49,50]. This strategy has recently been employed to assess the stabilization of the G4 structure following interaction with ligands, with results that are consistent with experimental data^[52]. Figure 3 presents the root-mean-square deviation (RMSD) values calculated for the entire G4 structure, its complex with **PL7**, and selected portions during the MD simulation performed at 300 K. To ascertain the stability of the **PL7/1KF1** complex, both the DNA atoms (shown in blue) and the ligand atoms (shown in yellow) were considered in RMSD simulations. The matching of the two RMSD values indicates that the ligand, once it is bounded, does not move significantly from its initial position, remaining stably linked to the G4. Moreover, the comparison of the RMSD between the free 1KF1 and **PL7/1KF1** indicates that the ligand induces stabilization, as evidenced by the slightly smaller RMSD values in its presence.

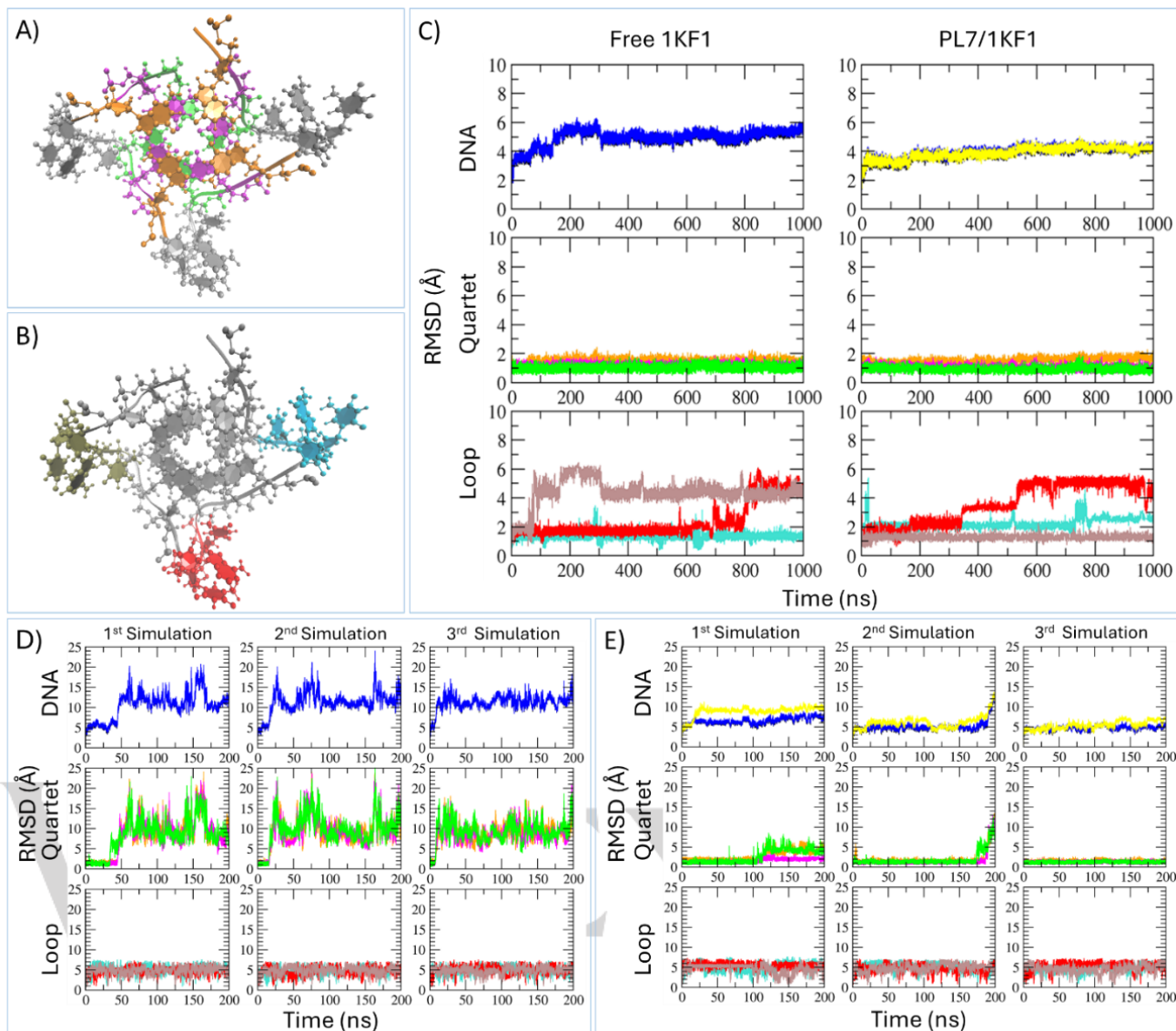


Figure 3. RMSD Results. (A) Color code used for quartets (B) Color code used for loops. These colors are the same used to indicate RMSD values. (C) RMSD calculated on: (top row) **1KF1** atoms except the first base in the 5' direction (blue), and **PL7/1KF1** atoms (yellow); (middle row) on each of the three G-quartets; (bottom row) on each of the three loops. Simulations conducted at 300K. (D) RMSDs calculated on three separate simulations at 525 K of free **1KF1**. (E) RMSDs calculated on three separate simulations at 525 K of **PL7/1KF1**.

This stabilization is primarily attributed to the enhanced stability of the loops. The simulations at higher temperatures confirm the stabilization effect of the ligand, as shown by the RMSD of the simulations performed at 525 K, shown in **Figure 3D** and **3E**. As expected, the RMSDs of the system at 525 K are in general higher than those at 300 K, however the behavior with and without the ligand is qualitatively very different. The RMSD of the loops reveal that these flexible portions do not keep their original organization at high temperature, either in absence or in presence of the ligand. However, the ligand has a strong effect on the stability of the G-quartets: in free **1KF1**, denaturation occurs within the first 50 ns. In the presence of PL7, denaturation is slower or not reached at all (**Figure 3E** - middle row), keeping the G4 structure stable. The simulations performed at 500 K and 550 K confirm the stabilizing effect of the ligand, as shown by the RMSD reported Figure S3.

Synthesized Oligonucleotides

The sequences used in the docking studies were taken as a starting point for choosing those to be used in the spectroscopic and spectrometric studies (Table 3). The sequence indicated by the acronym 23TAG (PDB ID: 2JSK^[53]) has been employed, corresponding to tandem repeats of the human telomeric region. This sequence in K⁺ solution leads to the folding of a form1/form2 hybrid topology G4, with a 70:30 ratio respectively^[54]. On the other hand, the modified sequences reported as CMA (PU19-A2A11^[55], PDB ID: 2LBY) and CMT (PU19-T2A11^[55]) are derived from the first 4 of 5 guanosine domains present in the NHEIII₁ region of the c-Myc gene^[44]. CMA and CMT tend to fold in parallel topology G4 in a K⁺ solution. This enabled the assessment of both the binding capacity and the selectivity of the proposed ligands toward G4 structures with different topologies.

Table 3. DNA oligonucleotide sequences

	1	2	3	4	5	6	7	8	9	10	11	12	13	14	15	16	17	18	19	20	21	22	23	
23TAG	5'-	T	A	G	G	G	T	T	A	G	G	T	T	A	G	G	G	T	T	A	G	G	G	-3'
CMA	5'-	T	A	G	G	G	A	G	G	G	T	A	G	G	G	A	G	G	G	T				-3'
CMT	5'-	T	T	G	G	G	A	G	G	G	T	A	G	G	G	A	G	G	G	T				-3'

Binding Constant UV-Visible Evaluation

UV-visible spectra of solutions of **TMPyP4** and **PL7** (Figure S8) were recorded upon addition of calf thymus DNA, 23TAG, and CMA, at 25 °C within the wavelength range of 200-800 nm. The porphyrins spectra typically exhibit a Soret band around 428 nm. Upon addition of DNA, in the **TMPyP4** solution, a red shift of the maximum absorption band was observed for the duplex, 23TAG, and CMA, with shifts of 2.3 nm, 2.1 nm, and 2.9 nm, respectively. Similarly, the red shifts observed for the **PL7** spectra amounted to 0.8 nm with duplex, 9.7 nm with 23TAG, and 5.8 nm with CMA. This red shift phenomenon is associated with a decrease in the energy of the $\pi \rightarrow \pi^*$ transition due to the interaction between the π -bonding orbital of the DNA base pairs and the empty π^* -antibonding orbital of the ligand. The hypochromic effect, determined by comparing absorbance maxima, is evidence of the interaction occurring between the nucleotides and porphyrins. The hypochromic effect (Table 4) increases in the order duplex < 23TAG < CMA with **TMPyP4** and in the order duplex < CMA < 23TAG with **PL7**, showing a difference compared to the duplex titration, of +9% (TAG23) and +5% (CMA). Binding constants could be determined by applying Benesi-Hildebrand method as reported in Supporting Information. The obtained values align with those documented in the literature^[56,57]. While **TMPyP4**, employed as a reference due to its well-established status, demonstrates binding constant values consistent across all studied DNA types (1.1 - $1.5 \times 10^6 M^{-1}$), **PL7** exhibits selectivity for the CMA sequence over the duplex, displaying a binding constant 2.6 times higher (Table 5).

Table 4. Red shift and hypochromicity

	TMPyP4		PL7	
	$\Delta\lambda$ (nm)	ΔA (%)	$\Delta\lambda$ (nm)	ΔA (%)
Duplex	2.3 ± 0.1	18 ± 2	0.8 ± 0.2	30 ± 2
23TAG	2.1 ± 0.4	22 ± 1	9.7 ± 0.5	39 ± 3
CMA	2.9 ± 0.5	24 ± 1	5.8 ± 0.3	35 ± 2

Calculated at porphyrin Soret band in presence of 0.5 μM DNA in spectroscopic titrations.

Table 5. Binding constants.

	Kb (M^{-1})	
	TMPyP4	PL7
Duplex	$(1.1 \pm 0.8) \times 10^6$	$(6.5 \pm 0.1) \times 10^5$
23TAG	$(1.5 \pm 0.4) \times 10^6$	$(6.1 \pm 0.3) \times 10^5$
CMA	$(1.5 \pm 0.6) \times 10^6$	$(1.7 \pm 0.4) \times 10^6$

NMR Study of Complex Structures

To assess interactions of herein synthesized porphyrin analogues with G4, 1H NMR monitored titration of 23TAG and CMA G4s were performed. These oligos differ slightly from the wild-type segments in order to increase the NMR spectral resolution in the imino-proton region without affecting the native structure. Notably, our studies were conducted in aqueous solutions at 20 mM K-phosphate, excluding KCl that reduces solubility of the herein studied porphyrin derivatives. Importantly, the acquired 1H NMR spectra of CMA and 23TAG folded in 20 mM K-phosphate without KCl, match literature reported spectra of G4 folded in the presence of 70/100 mM KCl^[44,54,58,59]. 1H NMR spectrum of CMA at 20 mM K-phosphate exhibits twelve imino signals in the range from δ 11.04 to 12.06 ppm, consistent with the formation of G4 with three G-quartets, i.e. G3→G7→G12→G16, G4→G8→G13→G17 and G5→G9→G14→G18, each comprising four Hoogsteen-type hydrogen-bonded guanine residues. Notably, the parallel-stranded topology of (free) CMA G4 relates to the core of the structure comprising guanine residues, which are connected with two single-residue (T6 and T15) and one two-residue (T10-A11) propeller-type loops, while overhangs on 5'- and 3'-ends consist of A1-T2 and T19, respectively. Upon addition of 0.5 mole equivalents of **PL7** the imino 1H NMR signals corresponding to the 'free CMA G4' became less intense and a new set of signals is observed in the range between 1H δ 10.08 and 11.02 ppm (Figure 4B).

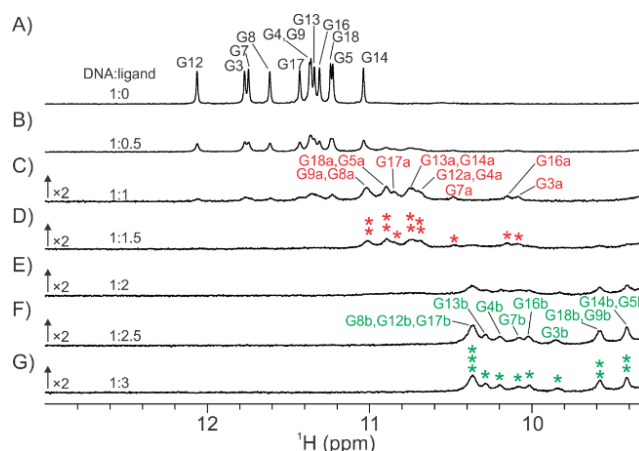


Figure 4. Imino region of the 1H NMR spectra of CMA G4 upon titration with **PL7**, whereby the molar ratios of DNA and the ligand are indicated above corresponding spectra. The signals corresponding to the 'free CMA G4', 'Complex a' and 'Complex b' are indicated with black, red, and green colors, respectively. Spectra were recorded at 0.2 mM DNA concentration, 25 °C in 90%/10% H_2O/H_2O , at 20 mM KPi, pH 7.0.

The new set of signals intensifies at 1:1 ratio of DNA:Ligand, consistent with the formation of a 1:1 binding stoichiometry complex called 'Complex a'. Moreover, at the equimolar concentrations of DNA and ligand there is an equilibrium

between 'free CMA G4' and 'Complex a' in a slight preference of the latter, while the species are in slow exchange on the ^1H NMR timescale at 600 MHz. ^1H NMR spectral analysis at 1.5 mole equivalents of **PL7** shows that intensity of signals corresponding to 'free CMA G4' decrease, while the 'Complex a' persists as the predominant species. NOESY and ROESY spectral analysis conducted at 1:1 DNA:ligand binding stoichiometry reveals cross-peaks arising from chemical exchange between 'free CMA G4' and 'Complex a', enabling assignment of new CMA imino chemical shifts influenced by the proximity of **PL7** (Figure 5 and Figure S5). Furthermore, comparison of imino ^1H NMR chemical shifts of free CMA G4 and 'Complex a' shows the largest perturbations for guanine residues at the 5'-end G-quartet, i.e. G3→G7→G12→G16, and the smallest for G5→G9→G14→G18 quartet at the 3'-end (Figure 5 and Figure S6). These results are consistent with 'Complex a' corresponding to CMA G4 exhibiting **PL7** stacked on the G3→G7→G12→G16 quartet and positioned proximal to the 5'-end overhanging residues T1 and A2 (Figure 5D). This is corroborated also by the observed ^1H NMR chemical shifts changes upon formation of 'Complex a' that are around 1.0 ppm for the methyl groups of T1 (located at the 5'-end). The fact that DNA-ligand NOE interactions are not resolved suggests that the binding is dynamic and involves exchange of the ligand between free- and bound-state and/or ligand reorientation at the binding site. Interestingly, at 2 mole equivalents of **PL7** ^1H NMR signals corresponding to 'Complex a' are reduced, while yet another set of signals appears between ^1H δ 9.4 and 10.4 ppm in line with the formation of 'Complex b', wherein CMA G4 and **PL7** interact at 1:2 binding stoichiometry (Figure 4E). ^1H NMR signals corresponding to 'Complex b' are further intensified at 2.5 mole equivalents of **PL7**, while precipitate is observed in the NMR sample at 3 (and higher) mole equivalents of the ligand with respect to 0.2 mM DNA, thus precluding further titration experiments. Notably, the slow exchange of 'Complex a' and 'Complex b' observed at 2 mole equivalents of **PL7** enabled identification of the corresponding NOESY and ROESY cross-peaks resulting from chemical exchange (Figure 5 and Figure S5). The analysis enabled assignment of imino ^1H NMR chemical shifts of CMA G4 within 'Complex b', furthermore allowing ^1H NMR chemical shift perturbation analysis showing that the 'Complex b' results upon **PL7** binding to the G5→G9→G14→G18 quartet at the 3'-end of the CMA G4 comprised in 'Complex a' (Figure 5D). In detail, comparison of imino ^1H NMR chemical shifts of 'Complex b' and 'Complex a' shows the largest differences for G5→G9→G14→G18 quartet at the 3'-end of the CMA G4, while the smallest ones for G3→G7→G12→G16 quartet at the 5'-end of the CMA G4. On the other hand, the $\Delta(\delta^1\text{H})$ for imino signals of 'Complex b' with respect to those for 'free CMA G4' show that differences are similar for the G3→G7→G12→G16 and G5→G9→G14→G18 quartets, in line with **PL7** stacked on both. Altogether, the NMR data is consistent with moderate to strong binding of **PL7** to CMA G4, whereby interactions comprise stacking of the ligand to the outer G-quartets, of which the 5'-end represents the preferential binding site.

Similar ^1H NMR studies were also extended to derivatives **PL7-Me** and **PL7-2Me** (Table 1), in which the amide hydrogens were replaced with 1 or 2 methyl groups respectively, to evaluate whether these structural modifications could modulate their

interaction capabilities. Study of interactions of CMA G4 with **PL7-Me** and **PL7-2Me** relied on the use of 1D and 2D NMR experiments analogous as described above for **PL7** (Figure S4). Upon addition of 0.5 to 1.5 molar equivalents of **PL7-Me** and **PL7-2Me** with respect to DNA, the ^1H NMR signals corresponding to 'free CMA G4' gradually became less intense and, in turn, a new set of signals is observed, consistent with the formation of 'Complex a' with ligand bound to the 5' end of CMA G4. Furthermore, no signals corresponding to DNA-ligand interactions were identified, whereas we observed cross-peaks in NOESY and ROESY spectra consistent with chemical exchange between 'free CMA G4' and 'Complex a'. Preferential binding of **PL7-Me** and **PL7-2Me** to the G3→G7→G12→G16 quartet is inferred from analyses of imino ^1H NMR chemical shift perturbation (Figure S6). Further additions to 2, 2.5 and 3 mole equivalents of **PL7-Me** or **PL7-2Me** with respect to CMA results in conversion of 'Complex a' into 'Complex b', in which ligands stack at both outer G-quartets of CMA G4 as inferred from the observed ^1H NMR chemical shift perturbations (Figure S6 and Table S1). Comparison of the ^1H NMR imino-protons chemical shift perturbations of CMA G4 upon binding of tetra-substituted porphyrins with different pendant groups shows very similar profiles, i.e. insignificant differences between **PL7** and **PL7-Me**, while slight variations are observed in the case of **PL7-2Me**. Most notable differences in ^1H NMR chemical shifts are observed when comparing 'Complex b' for **PL7-2Me** with respect to **PL7** and **PL7-Me**. Furthermore, the imino protons of G3, G7, G12, and G16 are shifted up field with $\Delta\delta$ of 0.24, 0.15, 0.19, and 0.25 ppm for **PL7-Me** vs. **PL7-2Me**; this suggest that dimethylated amide groups in **PL7-2Me** slightly interfere with G4 binding, probably by sterically hindering ligand interactions at the binding site comprising the 5'-end G3→G7→G12→G16 quartet. Considering that the G4 exhibits two 5'-end residues (T1-A2) while only one residue at the 3'-end (T19) where the preference of **PL7-2Me** binding is rather similar to **PL7** and **PL7-Me** suggests that binding relies not only on stacking of the ligands to G-quartets, but also on interactions between the ligand's pedant groups and overhanging residues. Consistent with this, extending the comparative analysis of ^1H NMR chemical shift perturbations to include NMR data on the binding of CMA G4 to the reference compound TMPyP4 (characterized by the shortest substituent on the pyridine nitrogen atom) shows that it binds slightly more strongly than **PL7**, **PL7-Me**, and **PL7-2Me** (Figure S6). To further explore binding of the herein studied porphyrin derivatives to G4 exhibiting different topologies we performed ^1H NMR-monitored titration of 23TAG, which at 20 mM KCl adopts G4 with hybrid-1 type topology while upon molecular crowding conditions induced by DMSO refolds into parallel-stranded G4^[18]. At diluted conditions and in the absence of ligand, ^1H NMR spectrum of 23TAG exhibits twelve major signals in the imino region characteristic for Hoogsteen-hydrogen bonded guanine residues, consistent with formation of the predominant G4 exhibiting hybrid type-1 topology (Figure S8 A). Additional broader ^1H NMR imino signals are observed corresponding to minor G4 forms present in the equilibrium. The ^1H NMR imino signals for both, the major and minor G4 forms decrease upon addition of 0.5 mole equivalent of the **PL7**. This effect is pronounced gradually at equimolar DNA and ligand concentrations as well as along the course of titration, whereby

at each of the analyzed DNA:Ligand ratios. Notably, the relative intensities of the imino ^1H NMR signals for the complex(es) change during titration. Hence, the NMR analysis suggests rather strong binding of the **PL7** to the parallel-stranded G4 adopted by 23TAG, which appears to exhibit multiple sites amenable to the ligand interactions. It is interesting to note that the 'free' 23TAG parallel G4 formed under crowding conditions is no longer observed at 1 mole equivalent of **PL7**, while the 'free' hybrid analogue persists even at 1:2 ratio between 23TAG and compound. These results are consistent with parallel G4 representing a better target for binding of **PL7**, whereby the interactions are aggravated by lateral loops in the hybrid topology, altogether stressing out the importance of the structural details related to the loops conformations with respect to the nearby (outer) G-quartets. The key role of residues extruded from the core of a G4 structure is further corroborated by the fact that shifting the equilibrium from parallel stranded G4 to complex formation requires 1.5 mole equivalents of **PL7** in the case of CMA (*vide supra*) (Figure 4), while only 1 mole equivalent in case of 23TAG (Figure S8 B). This suggests that **PL7** exhibits higher binding affinity for parallel G4 formed by 23TAG than for parallel G4 formed by CMA. The differences may relate to the different DNA-ligand interactions at the interfaces between overhanging or loop residues and pendant groups of the tetra-substituted porphyrins. In particular, parallel G4 adopted by 23TAG exhibits three-residue propeller-type loops, while in the case of CMA the propeller-type loops comprise only one or two residues. The longer loops in case of 23TAG with respect to CMA exhibit more flexibility, which potentially guides and facilitates binding of the **PL7**. Analogously, longer pendant groups of tetra-substituted porphyrins may promote G4 binding, which is substantiated by the results of comparative ^1H NMR.

Circular Dichroism

To further confirm the selectivity of **PL7** for the parallel topology, circular dichroism analyses were performed. As can be seen from Figure 6A, the spectrum of the CMA sequence shows a shape characteristic for parallel topology, with a positive band around 260 nm and a negative one at 240 nm. No changes in bands position were observed after either **TMPyP4** or **PL7** titrations, which confirms the retention of the parallel topology (Figure 6A). The spectrum of free 23TAG (Figure 6B) shows a characteristic hybrid topology pattern, i.e., a positive band at 290 nm. Again, the G4 was subjected to titrations with 1.5 equivalents of **TMPyP4** or **PL7**: in contrast to CMA, with 23TAG there is a change in the spectra for both titrations, showing a decrease in the intensity of the band at 290 nm and an increase at 260 nm. This effect indicates further confirmation that porphyrin ligands show selectivity for parallel topology. If this is not present, as in the case of 23TAG, they stimulate refolding by activating structural equilibria. These underlie the failure to isolate the complex via NMR for the sequence with hybrid topology.

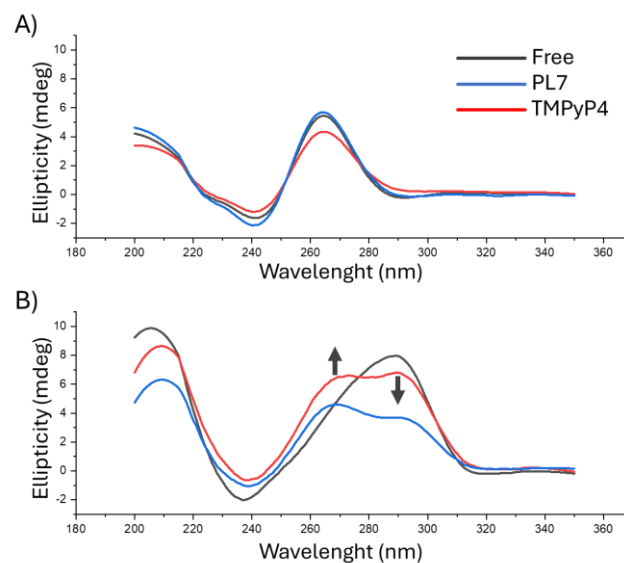


Figure 6. Circular dichroism spectra of (A) CMA and (B) 23TAG in diluted conditions. The spectra were recorded at 25 °C in 90%/10% $\text{H}_2\text{O}/^2\text{H}_2\text{O}$, at 20 mM KPi, pH 7.0- and 0.2-mM DNA. **TMPyP4** and **PL7** were added in 1.5 eq.

Mass Spectrometry

Mass spectrometry proves to be an efficient technique in assessing the stability of complexes formed by nucleic acids^[46]. In our case, the analyses were conducted using a mass spectrometer with an ESI source, as reported in the experimental section. The primary advantage of electrospray ionization mass spectrometry is its capability to transfer analytes of interest from the sample solution to the mass spectrometer with minimal fragmentation. A common strategy for enhancing the ion response in ESI-MS is to add organic co-solvents that are more volatile than water, such as MeOH^[60]. This phenomenon arises from the ability of methanol to reduce the surface tension of droplets, thereby promoting droplet formation, fission, and evaporation processes. As reported by Rosu *et al.*, the use of a specific methanol concentration not only results in a substantial increase in signal but also minimizes potential conformational alterations in solution^[46]. Therefore, an 8:2 H_2O :MeOH solution was used to dilute stock solution to bring sequence concentration to 15 μM . The sequences employed for these experiments were 23TAG and CMT. CMT corresponds to CMA, with the distinction that in CMT, the second guanine has been replaced by thymine. As already reported^[44], NMR studies conducted on this sequence reveal that both the CMA and CMT G4 share common structural characteristics. These include a core comprised of three G-quartets, three propeller-type loops, and a T19 residue located at the 3'-end overhang. Since the fundamental folding topologies of the CMA and CMT G4 remain unaltered even when subjected to a single A-T nucleotide substitution at the 5'-end, CMT has been used for mass experiments instead of CMA. The stabilizing activity of **TMPyP4**, **PL7**, **PL7-Me** and **PL7-2Me** was evaluated by MS/MS using the collision-induced dissociation (CID) technique. The latter involves isolating the molecular ion in a collision chamber and gradually increasing the collision energy until the target peak disappears. From these experiments, it was possible to calculate the energy required for dissociation of the complex peak to its relative half-intensity ($E_{\text{COM}}^{50\%}$)^[61] using the relative intensities of the target ions from Equation (1).

$$(1) \quad \text{relative intensity} = \frac{I_{\text{Target Ion}}}{I_{\text{Target Ion}} + I_{\text{Dissociation Products}}}$$

Mass spectrometry is less sensitive to structural equilibria than NMR spectroscopy making possible to isolate complexes with the 23TAG. This supports the thesis that the reduction in intensity of the imino ^1H NMR signals observed during titrations of G4 with ligands is due to the formation of a complex. However, no Complex b at a G4:ligand ratio of 1:2 has been isolated, suggesting that one of the two terminal G-quartets of hybrid G4 is sterically hindered, impeding the stacking of the ligand. Complex b was isolated with CMT G4 using **TMPyP4** and **PL7**. Table 6 summarizes the results of the stability studies. Overall, the proposed ligands stabilize both CMT and 23TAG sequences. For CMT, both **PL7** and **TMPyP4** show an increase in stability from Complex a to Complex b. Additionally, from the $E_{\text{COM}^{50\%}}$ values, it is evident that an increase in the number of ligands present is directly proportional to an increase in G4 stability. However, it's important to note that this is not a trivial observation, as excessive ligand binding capacity can lead to destabilization and subsequent unfolding of the G4 structure.

Table 6. $E_{\text{COM}^{50\%}}$ values

Oligonucleotide	Ligand	$E_{\text{COM}^{50\%}}$ G4 (eV)
23TAG	No ligand	28.9
	TMPyP4 ^[a]	38.5
	PL7 ^[a]	38.8
	PL7-Me ^[a]	39.6
	PL7-2Me ^[a]	40.2
CMT	No ligand	26.5
	TMPyP4 ^[a]	35.9
	TMPyP4 ^[b]	48.5
	PL7 ^[a]	35.9
	PL7 ^[b]	45.5

[a] Complex a with 1:1 stoichiometry. [b] Complex b with 1:2 stoichiometry.

Proliferation assay

An MTT assay was conducted on MCF-7 cell lines, using **PL7** and **TMPyP4** porphyrins. The investigation aimed to assess the potential cytotoxic effects of these porphyrins on cancerous cell lines. The results (Figure 7) of the MTT assay unveiled a compelling dose-response relationship for both **PL7** and **TMPyP4**, revealing their impact on cell viability. Notably, **PL7** exhibited an IC_{50} value of 3.265 μM , indicating its potency in inhibiting cell proliferation. Also in this case, as for NMR experiments, results are comparable with once obtained for **TMPyP4**, that shows an IC_{50} of 3.651 μM . These findings showed that both molecules were able to induce a stop in the cell growth at relatively low concentrations.

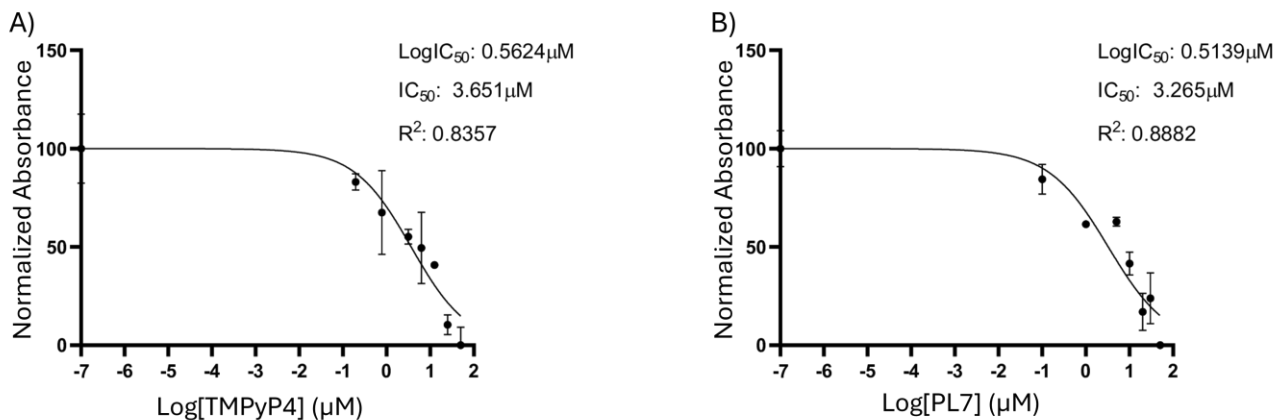


Figure 7. IC_{50} from the MTT assay on MCF-7 cell line with A) **TMPyP4** and B) **PL7**. The x-axis represents the logarithm of the concentration while the y-axis contains the % of living cells in the sample.

Conclusion

A series of cationic porphyrins were designed and their interaction with different G4s was evaluated. An initial molecular docking study identified the most promising ligands based on their interaction energies with G4s of different nature and topology. The calculations showed parallel topology as most preferred and **PL7** as the most promising derivative. In addition **PL7** stabilizing ability was then evaluated by an extensive set of MD simulations of the telomeric parallel G4 in presence and absence of the ligand. The simulations were performed both at room temperature (300 K) and at higher temperature (500, 525 and 500 K) and indicated a stabilizing effect of **PL7** on the G4 structure. Considering these results, **PL7** and **TMPyP4** were synthesized, and binding constant evaluated on calf thymus (duplex), 23TAG (hybrid G4 from human telomeres) and CMA (parallel G4 from c-Myc) by UV-Visible titrations. While **TMPyP4** showed no selectivity, **PL7** shows a 3-fold preference for parallel G4 over duplex and hybrid G4. NMR spectroscopy was used to study the structures of the **PL7**/G4 complexes, again showing that the G4 CMA is preferred due to its topology. Circular dichroism analyses suggested that while in the case of all parallel G4s there is no effect beyond coordination on the quartets, in the case of hybrid G4s there was a structural change induced by the presence of the ligand, which drives it to refold in the parallel topology, triggering structural equilibria that do not allow NMR study. Molecular crowding conditions were tested on the 23TAG sequence to drive its folding in parallel topology. ¹H NMR-monitored titration of G4 with **PL7** shows appearance of a new set of signals consistent with the formation of DNA/ligand complex(es). The interaction of the amide groups with the loops of G4 was not identified by NMR, suggesting a dynamic coordination on the quartets. Analysis of the differences in imino ¹H NMR chemical shifts for CMA G4 in complexes with **PL7-Me** and **PL7-2Me** shows that the presence of at least one potential hydrogen bond donor in the ligand's pendant group balances the larger steric hindrance, which partially disfavors stacking on the quartets. Mass spectrometry collision-induced dissociation experiments on 23TAG and CMA complexes with **TMPyP4** and **PL7** have shown very similar stabilizing effects. Finally, preliminary cytotoxicity assays were performed on a breast cancer cell line in which the IC₅₀ values obtained for **TMPyP4** and **PL7** are comparable. This study was able to confirm the propensity of porphyrin ligands for parallel G4, a topology preferred under the naturally occurring conditions of molecular crowding in the cellular environment. **PL7** demonstrated how the presence of amide groups gives a balance of steric hindrance and dipolar interaction with loops, that improves selectivity for parallel G4s over other structures. Considering also the easy of synthesis, **PL7** could be regarded as a better alternative to **TMPyP4** in studies involving G4 binding.

Supporting Information

The authors have cited additional references within the Supporting Information.^[62-107]

Acknowledgements

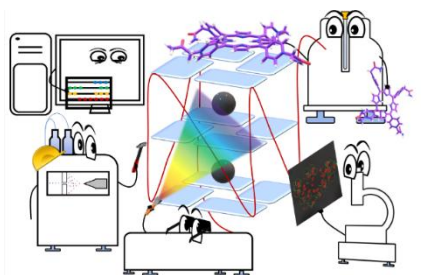
FM acknowledges the National Supercomputer Center (Naiss) in Sweden for the computational resource and Fondazione Banco di Sardegna (FDS) (grant number F73C23001600007) for funding. Simone Mulliri, Elisabetta Cardinale and Fabio Esposito are kindly acknowledged for performing the docking for ligands **PL6** and **PL7**. JP and MT thank the Slovenian Research and Innovation Agency [P1-0242, J1- 1704]. The authors would like to thank CERIC-ERIC consortium for the access to experimental facilities and financial support (grant No. 20232091). This work was financially supported by Regione Autonoma della Sardegna within the project "Green Chemistry" in "Drug Discovery: sintesi sostenibili di nuovi inibitori di telomerasi" (RASSR81788-Bando "Invito a presentare progetti di ricerca di base – Annualità 2017")

Keywords: DNA • G-quadruplexes • Molecular dynamics • Molecular recognition • NMR

- [1] M. L. Bochman, K. Paeschke, V. A. Zakian, *Nat. Rev. Genet.* **2012**, *13*, 770–780.
- [2] D. Yang, C. Lin, Eds., *G-Quadruplex Nucleic Acids: Methods and Protocols*, Springer New York, New York, NY, **2019**.
- [3] L. Hayflick, P. S. Moorhead, *Exp. Cell Res.* **1961**, *25*, 585–621.
- [4] A. G. Bodnar, M. Ouellette, M. Frolkis, S. E. Holt, C. P. Chiu, G. B. Morin, C. B. Harley, J. W. Shay, S. Lichtsteiner, W. E. Wright, *Science* **1998**, *279*, 349–352.
- [5] J. W. Shay, W. E. Wright, *Semin. Cancer Biol.* **2011**, *21*, 349–353.
- [6] N. W. Kim, M. A. Piatyszek, K. R. Prowse, C. B. Harley, M. D. West, P. L. C. Ho, G. M. Coviello, W. E. Wright, S. L. Weinrich, J. W. Shay, *Science* **1994**, *266*, 2011–2015.
- [7] C. Bryan, C. Rice, H. Hoffman, M. Harkisheimer, M. Sweeney, E. Skordalakes, *Structure* **2015**, *23*, 1934–1942.
- [8] A. Asai, Y. Oshima, Y. Yamamoto, T. Uochi, H. Kusaka, S. Akinaga, Y. Yamashita, K. Pongracz, R. Pruzan, E. Wunder, M. Piatyszek, S. Li, A. C. Chin, C. B. Harley, S. Gryaznov, *Cancer Res.* **2003**, *63*, 3931–3939.
- [9] N. Kosiol, S. Juranek, P. Brossart, A. Heine, K. Paeschke, *Mol. Cancer* **2021**, *20*, 40.
- [10] S. Balasubramanian, S. Neidle, *Curr. Opin. Chem. Biol.* **2009**, *13*, 345–353.
- [11] C. Hennecker, L. Yamout, C. Zhang, C. Zhao, D. Hiraki, N. Moitessier, A. Mittermaier, *Int. J. Mol. Sci.* **2022**, *23*, 16020.
- [12] S. Da Ros, G. Nicoletto, R. Rigo, S. Ceschi, E. Zorzan, M. Dacasto, M. Giantin, C. Sissi, *Int. J. Mol. Sci.* **2021**, *22*, 329.
- [13] S. A. Miller, J. Nandi, N. E. Leadbeater, N. A. Eddy, *Eur. J. Org. Chem.* **2020**, *2020*, 108–112.
- [14] V. González, L. H. Hurley, *Biochemistry* **2010**, *49*, 9706–9714.
- [15] A. Siddiqui-Jain, C. L. Grand, D. J. Bearss, L. H. Hurley, *Proc. Natl. Acad. Sci. U. S. A.* **2002**, *99*, 11593–11598.
- [16] J. Spiegel, S. Adhikari, S. Balasubramanian, *Trends Chem.* **2020**, *2*, 123–136.
- [17] D. Miyoshi, N. Sugimoto, *Biochimie* **2008**, *90*, 1040–1051.
- [18] B. Heddi, A. T. Phan, *J. Am. Chem. Soc.* **2011**, *133*, 9824–9833.
- [19] T. Fujii, P. Podbevšek, J. Plavec, N. Sugimoto, *J. Inorg. Biochem.* **2017**, *166*, 190–198.
- [20] V. Viglasky, T. Hianik, *Gen. Physiol. Biophys.* **2013**, *32*, 149–172.
- [21] T. Troha, I. Drevensšek-Olenik, M. Webba da Silva, L. Spindler, *Langmuir* **2016**, *32*, 7056–7063.
- [22] F. C. Simmel, W. U. Dittmer, *Small* **2005**, *1*, 284–299.
- [23] K. Shin-ya, K. Wierzbka, K. Matsuo, T. Ohtani, Y. Yamada, K. Furihata, Y. Hayakawa, H. Seto, *J. Am. Chem. Soc.* **2001**, *123*, 1262–1263.
- [24] S. M. Gowan, J. R. Harrison, L. Patterson, M. Valenti, M. A. Read, S. Neidle, L. R. Kelland, *Mol. Pharmacol.* **2002**, *61*, 1154–1162.
- [25] W. J. Chung, B. Heddi, M. Tera, K. Iida, K. Nagasawa, A. T. Phan, *J. Am. Chem. Soc.* **2013**, *135*, 13495–13501.
- [26] F. Hamon, E. Largy, A. Guédin-Beaupaire, M. Rouchon-Dagois, A. Sidibe, D. Monchaud, J.-L. Mergny, J.-F. Riou, C.-H. Nguyen, M.-P. Teulade-Fichou, *Angew. Chem. Int. Ed.* **2011**, *50*, 8745–8749.
- [27] S. Balasubramanian, L. H. Hurley, S. Neidle, *Nat. Rev. Drug Discov.* **2011**, *10*, 261–275.
- [28] A. De Cian, E. DeLemos, J.-L. Mergny, M.-P. Teulade-Fichou, D. Monchaud, *J. Am. Chem. Soc.* **2007**, *129*, 1856–1857.
- [29] A. Terenzi, H. Gattuso, A. Spinello, B. K. Keppler, C. Chipot, F. Dehez, G. Barone, A. Monari, *Antioxidants* **2019**, *8*, 472.
- [30] A. Criscuolo, E. Napolitano, C. Riccardi, D. Musumeci, C. Platella, D. Montesarchio, *Pharmaceutics* **2022**, *14*, 2361.

- [31] S. Asamitsu, S. Obata, Z. Yu, T. Bando, H. Sugiyama, *Molecules* **2019**, *24*, 429.
- [32] S. Pelliccia, J. Amato, D. Capasso, S. Di Gaetano, A. Massarotti, M. Piccolo, C. Irace, G. C. Tron, B. Pagano, A. Randazzo, E. Novellino, M. Giustiniano, *J. Med. Chem.* **2020**, *63*, 2035–2050.
- [33] S. Neidle, Ed., *Quadruplex Nucleic Acids as Targets for Medicinal Chemistry*, AP, Academic Press, An Imprint Of Elsevier, Cambridge, MA San Diego, CA Kidlington, Oxford London, **2020**.
- [34] M. Ghahremani Nasab, L. Hassani, S. Mohammadi Nejad, D. Norouzi, *J. Biol. Phys.* **2017**, *43*, 5–14.
- [35] R. T. Wheelhouse, D. Sun, H. Han, F. X. Han, L. H. Hurley, *J. Am. Chem. Soc.* **1998**, *120*, 3261–3262.
- [36] C. L. Grand, H. Han, R. M. Muñoz, S. Weitman, D. D. Von Hoff, L. H. Hurley, D. J. Bearss, *Mol. Cancer Ther.* **2002**, *1*, 565–573.
- [37] J. Ren, J. B. Chaires, *Biochemistry* **1999**, *38*, 16067–16075.
- [38] I. M. Dixon, F. Lopez, J.-P. Estève, A. M. Tejera, M. A. Blasco, G. Pratiel, B. Meunier, *ChemBioChem* **2005**, *6*, 123–132.
- [39] I. M. Dixon, F. Lopez, A. M. Tejera, J.-P. Estève, M. A. Blasco, G. Pratiel, B. Meunier, *J. Am. Chem. Soc.* **2007**, *129*, 1502–1503.
- [40] Y. Du, D. Zhang, W. Chen, M. Zhang, Y. Zhou, X. Zhou, *Bioorg. Med. Chem.* **2010**, *18*, 1111–1116.
- [41] A. Ferino, G. Nicoletto, F. D'Este, S. Zorzet, S. Lago, S. N. Richter, A. Tikhomirov, A. Shchekotikhin, L. E. Xodo, *J. Med. Chem.* **2020**, *63*, 1245–1260.
- [42] G. N. Parkinson, M. P. H. Lee, S. Neidle, *Nature* **2002**, *417*, 876–880.
- [43] A. Ambrus, D. Chen, J. Dai, R. A. Jones, D. Yang, *Biochemistry* **2005**, *44*, 2048–2058.
- [44] M. Trajkovski, E. Morel, F. Hamon, S. Bombard, M.-P. Teulade-Fichou, J. Plavec, *Chem. – Eur. J.* **2015**, *21*, 7798–7807.
- [45] M. Adrian, B. Heddi, A. T. Phan, *Methods* **2012**, *57*, 11–24.
- [46] F. Rosu, E. De Pauw, V. Gabelica, *Biochimie* **2008**, *90*, 1074–1087.
- [47] G. Ribaud, A. Ongaro, G. Zagotto, M. Memo, A. Gianoncelli, *Nat. Prod. Res.* **2021**, *35*, 2583–2587.
- [48] V. Gabelica, *Acc. Chem. Res.* **2021**, *54*, 3691–3699.
- [49] R. Day, B. J. Bennion, S. Ham, V. Daggett, *J. Mol. Biol.* **2002**, *322*, 189–203.
- [50] D. O. Alonso, E. Alm, V. Daggett, *Structure* **2000**, *8*, 101–110.
- [51] G. Todde, S. Hovmöller, A. Laaksonen, F. Mocchi, *Proteins Struct. Funct. Bioinforma.* **2014**, *82*, 2353–2363.
- [52] S. Mulliri, A. Laaksonen, P. Spanu, R. Farris, M. Farci, F. Mingoia, G. N. Roviello, F. Mocchi, *Int. J. Mol. Sci.* **2021**, *22*, 6028.
- [53] A. T. Phan, V. Kuryavyy, K. N. Luu, D. J. Patel, *Nucleic Acids Res.* **2007**, *35*, 6517–6525.
- [54] K. N. Luu, A. T. Phan, V. Kuryavyy, L. Lacroix, D. J. Patel, *J. Am. Chem. Soc.* **2006**, *128*, 9963–9970.
- [55] R. I. Mathad, E. Hatzakis, J. Dai, D. Yang, *Nucleic Acids Res.* **2011**, *39*, 9023–9033.
- [56] T. Santos, J. Lopes-Nunes, D. Alexandre, A. Miranda, J. Figueiredo, M. S. Silva, J.-L. Mergny, C. Cruz, *Biochimie* **2022**, *200*, 8–18.
- [57] C. Wei, J. Wang, M. Zhang, *Biophys. Chem.* **2010**, *148*, 51–55.
- [58] R. I. Mathad, E. Hatzakis, J. Dai, D. Yang, *Nucleic Acids Res.* **2011**, *39*, 9023–9033.
- [59] A. T. Phan, V. Kuryavyy, K. N. Luu, D. J. Patel, *Nucleic Acids Res.* **2007**, *35*, 6517–6525.
- [60] R. Ferreira, A. Marchand, V. Gabelica, *Methods* **2012**, *57*, 56–63.
- [61] M. Torvinen, E. Kalenius, F. Sansone, A. Casnati, J. Jänis, *J. Am. Soc. Mass Spectrom.* **2012**, *23*, 359–365.
- [62] “Computational Platform for Molecular Discovery & Design,” can be found under <https://www.schrodinger.com/platform/> (accessed 2024-04-15).
- [63] “Life Science: Maestro,” can be found under <https://www.schrodinger.com/platform/products/maestro/> (accessed 2024-04-15).
- [64] “2D Sketcher,” can be found under <https://www.schrodinger.com/platform/products/schrodinger-2d-sketcher/> (accessed 2024-04-15).
- [65] “Schrodinger Release 2024-1: LigPrep, Schrodinger, LLC, New York, NY, 2024,” can be found under <https://www.schrodinger.com/platform/products/ligprep/> (accessed 2024-04-15).
- [66] J. Dai, M. Carver, C. Punchihewa, R. A. Jones, D. Yang, *Nucleic Acids Res.* **2007**, *35*, 4927–4940.
- [67] Y. Wang, D. J. Patel, *Structure* **1993**, *1*, 263–282.
- [68] J. C. Shelley, A. Cholleti, L. L. Frye, J. R. Greenwood, M. R. Timlin, M. Uchimaya, *J. Comput. Aided Mol. Des.* **2007**, *21*, 681–691.
- [69] E. Harder, W. Damm, J. Maple, C. Wu, M. Reboul, J. Y. Xiang, L. Wang, D. Lupyan, M. K. Dahlgren, J. L. Knight, J. W. Kaus, D. S. Cerutti, G. Krilov, W. L. Jorgensen, R. Abel, R. A. Friesner, *J. Chem. Theory Comput.* **2016**, *12*, 281–296.
- [70] W. L. Jorgensen, D. S. Maxwell, J. Tirado-Rives, *J. Am. Chem. Soc.* **1996**, *118*, 11225–11236.
- [71] R. A. Friesner, J. L. Banks, R. B. Murphy, T. A. Halgren, J. J. Klicic, D. T. Mainz, M. P. Repasky, E. H. Knoll, M. Shelley, J. K. Perry, D. E. Shaw, P. Francis, P. S. Shenkin, *J. Med. Chem.* **2004**, *47*, 1739–1749.
- [72] T. A. Halgren, R. B. Murphy, R. A. Friesner, H. S. Beard, L. L. Frye, W. T. Pollard, J. L. Banks, *J. Med. Chem.* **2004**, *47*, 1750–1759.
- [73] R. A. Friesner, R. B. Murphy, M. P. Repasky, L. L. Frye, J. R. Greenwood, T. A. Halgren, P. C. Sanschagrin, D. T. Mainz, *J. Med. Chem.* **2006**, *49*, 6177–6196.
- [74] R. Galindo-Murillo, J. C. Robertson, M. Zgarbová, J. Šponer, M. Otyepka, P. Jurečka, T. E. I. Cheatham, *J. Chem. Theory Comput.* **2016**, *12*, 4114–4127.
- [75] J. Šponer, G. Bussi, P. Stadlbauer, P. Kührová, P. Banáš, B. Islam, S. Haider, S. Neidle, M. Otyepka, *Biochim. Biophys. Acta Gen. Subj.* **2017**, *1861*, 1246–1263.
- [76] A. Atzori, S. Liggj, A. Laaksonen, M. Porcu, A. P. Lyubartsev, G. Saba, F. Mocchi, *Can. J. Chem.* **2016**, *94*, 1181–1188.
- [77] M. Havrila, P. Stadlbauer, B. Islam, M. Otyepka, J. Šponer, *J. Chem. Theory Comput.* **2017**, *13*, 3911–3926.
- [78] F. Mocchi, A. Laaksonen, *Soft Matter* **2012**, *8*, 9268–9284.
- [79] M. Rebić, A. Laaksonen, J. Šponer, J. Uličný, F. Mocchi, *J. Phys. Chem. B* **2016**, *120*, 7380–7391.
- [80] M. Krepl, M. Zgarbová, P. Stadlbauer, M. Otyepka, P. Banáš, J. Koča, T. E. Cheatham, P. Jurečka, J. Šponer, *J. Chem. Theory Comput.* **2012**, *8*, 2506–2520.
- [81] M. Zgarbová, J. Šponer, M. Otyepka, T. E. Cheatham, R. Galindo-Murillo, P. Jurečka, *J. Chem. Theory Comput.* **2015**, *11*, 5723–5736.
- [82] A. Pérez, I. Marchán, D. Svozil, J. Šponer, T. E. Cheatham, C. A. Laughton, M. Orozco, *Biophys. J.* **2007**, *92*, 3817–3829.
- [83] M. Zgarbová, F. J. Luque, J. Šponer, T. E. Cheatham, M. Otyepka, P. Jurečka, *J. Chem. Theory Comput.* **2013**, *9*, 2339–2354.
- [84] W. D. Cornell, P. Cieplak, C. I. Bayly, I. R. Gould, K. M. Merz, D. M. Ferguson, D. C. Spellmeyer, T. Fox, J. W. Caldwell, P. A. Kollman, *J. Am. Chem. Soc.* **1995**, *117*, 5179–5197.
- [85] J. Wang, W. Wang, P. A. Kollman, D. A. Case, *J. Mol. Graph. Model.* **2006**, *25*, 247–260.
- [86] I. Rajasingh, B. Rajan, R. S. Rajan, *Appl. Math.* **2010**, *01*, 499–503.
- [87] C. Komenan, *Adv. Lit. Study* **2019**, *07*, 176–192.
- [88] E. Görg, *Adv. Hist. Stud.* **2014**, *03*, 56–67.
- [89] M. R. Farahani, W. Gao, *Appl. Math.* **2015**, *06*, 2319–2325.
- [90] F. G. Alvarenga, M. J. S. Houndjo, A. V. Monwanou, J. B. C. Orou, *J. Mod. Phys.* **2013**, *04*, 130–139.
- [91] C. I. Bayly, P. Cieplak, W. Cornell, P. A. Kollman, *J. Phys. Chem.* **1993**, *97*, 10269–10280.
- [92] J. Wang, R. M. Wolf, J. W. Caldwell, P. A. Kollman, D. A. Case, *J. Comput. Chem.* **2004**, *25*, 1157–1174.
- [93] H. J. C. Berendsen, J. R. Grigera, T. P. Straatsma, *J. Phys. Chem.* **1987**, *91*, 6269–6271.
- [94] I. S. Joung, T. E. I. Cheatham, *J. Phys. Chem. B* **2009**, *113*, 13279–13290.
- [95] I. S. Joung, T. E. I. Cheatham, *J. Phys. Chem. B* **2008**, *112*, 9020–9041.
- [96] R. Salomon-Ferrer, D. A. Case, R. C. Walker, *WIREs Comput. Mol. Sci.* **2013**, *3*, 198–210.
- [97] D. A. Case, T. E. Cheatham, T. Darden, H. Gohlke, R. Luo, K. M. Merz, A. Onufriev, C. Simmerling, B. Wang, R. J. Woods, *J. Comput. Chem.* **2005**, *26*, 1668–1688.
- [98] D. A. Pearlman, D. A. Case, J. W. Caldwell, W. S. Ross, T. E. Cheatham, S. DeBolt, D. Ferguson, G. Seibel, P. Kollman, *Comput. Phys. Commun.* **1995**, *91*, 1–41.
- [99] H. J. C. Berendsen, J. P. M. Postma, W. F. van Gunsteren, J. Hermans, in *Intermolecular Forces Proc. Fourteenth Jerus. Symp. Quantum Chem. Biochem. Held Jerus. Isr. April 13–16 1981* (Ed.: B. Pullman), Springer Netherlands, Dordrecht, **1981**, pp. 331–342.
- [100] J.-P. Ryckaert, G. Ciccoliti, H. J. C. Berendsen, *J. Comput. Phys.* **1977**, *23*, 327–341.
- [101] T. Darden, D. York, L. Pedersen, *J. Chem. Phys.* **1993**, *98*, 10089–10092.
- [102] G. Todde, S. Hovmöller, A. Laaksonen, F. Mocchi, *Proteins* **2014**, *82*, 2353–2363.
- [103] R. Day, B. J. Bennion, S. Ham, V. Daggett, *J. Mol. Biol.* **2002**, *322*, 189–203.
- [104] D. O. Alonso, E. Alm, V. Daggett, *Struct. Lond. Engl.* **1993** **2000**, *8*, 101–110.
- [105] G. Magdy, F. Belal, A. F. Abdel Hakiem, A. M. Abdel-Megied, *Int. J. Biol. Macromol.* **2021**, *182*, 1852–1862.
- [106] A. S. Levenson, V. C. Jordan, *Cancer Res.* **1997**, *57*, 3071–3078.
- [107] T. Mosmann, *J. Immunol. Methods* **1983**, *65*, 55–63.

Entry for the Table of Contents



Molecular docking and dynamics and multiple spectroscopic and spectrometric determinations allowed us to monitor interaction with different DNA sequences of simple cationic porphyrins. 5,10,15,20-tetrakis-(1-acetamido-4-pyridyl)porphyrin bromide in particular demonstrated a better selectivity compared to tetramethylpyridylporphyrin in binding G-quadruplex with parallel topology compared with hybrid and with duplex forming oligonucleotides.

Institute and/or researcher Twitter usernames: @unissTweet @MCarraroUniss